Two types of highly efficient electrostatic traps for single loading or multi-loading of polar molecules[*]

Bin Wei(魏斌), Hengjiao Guo(郭恒娇), Yabing Ji(纪亚兵), Shunyong Hou(侯顺永)[†], and Jianping Yin(印建平)[‡]

State Key Laboratory of Precision Spectroscopy, East China Normal University, Shanghai 200062, China

Two novel electrostatic traps named octopole-based disk electrostatic trap (ODET) and tubular-based disk electrostatic trap (TDET) are proposed for trapping cold polar molecules in low-field-seeking states. Using MgF as the target molecule, single loading and multi-loading methods are numerically simulated with varied incident velocities of slow molecular beams in the two types of traps, respectively. In ODET, with an incident velocity of 10 m/s, a highest loading efficiency of 78.4% or 99.9% has been achieved under the single loading or multi-loading operation mode. In TDET, with an incident velocity of 11 m/s, a highest loading efficiency of 81.6% or 106.5% has been achieved using the two loading methods, respectively. With such high loading efficiencies, the trapped cold molecules can be applied in the researches of cold collisions, high precision spectroscopy, and precision measurements. Especially, together with a blue-detuned hollow beam, the new electrostatic traps proposed here offer a new platform for the following gradient-intensity cooling of MgF molecules, which may provide a new way to produce high density ultracold molecules.

1. Introduction

Research on cold molecules is progressing rapidly, which offers unique possibilities for the investigation of new physical phenomena.[1–3] The trapped cold molecules especially are suitable for or facilitate the study of cold collisions,[4–7] cold chemistry,[8–11] high-resolution spectroscopy,[12,13] and precision measurements,[14–16] benefiting from the longer observation time. A variety of techniques have been developed to trap cold molecules.[17–27] In 1998, Doyle group realized magnetic trapping of calcium monohydride molecules thermalized in helium buffer gas.[28] In the same year, Knize group successfully trapped cesium dimers with an optical trap.[29] In 2000, Meijer group demonstrated electrostatic trapping of ammonia molecules with a trap that composes of two end-caps and a ring electrode in the middle.[30] Thus far, several cold species of interest and highly relevant to science are trapped with electric or magnetic fields, including ND_3 molecules,[18–20,22,30] OH radicals,[21,31] metastable CO molecules,[32] and NH radicals,[33–35] which have been used in the studies of direct measurement of the radiative lifetime,[32,36] cold collisions,[37–39] nonadiabatic transitions,[22] Zeeman relaxation,[34] and Sisyphus cooling.[40] Generally, the trap mentioned above is loaded in a single cycle, which obviously limits the number of the trapped molecules and thus the number density. A sufficient number in the trap is absolutely essential for the study of molecular

collisions and future applications such as evaporative or sympathetic cooling. In 2001, van de Meerakker *et al.* proposed a subtle method that works specifically for NH radicals to accumulate the molecules decelerated by a Stark decelerator in a magnetic trap to increase the phase-space density,[41] and it was experimentally demonstrated in 2011.[42] In 2005, Rempe group realized a continuously loading of an electrostatic trap for ND_3 molecules from a quadrupole velocity filter, where the trap consists of five ring-shaped electrodes and two spherical electrodes at both ends.[43]

Here, we propose two types of highly efficient electrostatic traps for trapping polar molecules. With the single loading method, the slow molecules are loaded in one cycle, during which the trap potential is kept switching on. With the multi-loading method, the molecules are loaded in five cycles, and the trap potential requires opening up after each cycle. Throughout the paper, we choose MgF as the target molecule, as it is feasible for laser cooling.[44–46] Furthermore, the electrostatic trapped MgF molecules are anticipated to be used in the gradient-intensity cooling with a blue-detuned hollow beam, which may provide a new approach to produce dense ultracold molecules.

In the following sections, the geometries of the new traps and the electric distributions generated by the electrodes of the traps are presented. In order to verify the loading methods, Monte Carlo simulations are performed for the two types of

[†]Corresponding author. E-mail: syhou@lps.ecnu.edu.cn

[‡]Corresponding author. E-mail: jpyin@phy.ecnu.edu.cn

traps operated with the single loading and the multi-loading methods, respectively. The resulting phase-space distributions and velocity distributions are also given. Some discussion and conclusions are presented at the end.

2. Trap schemes

2.1. Octopole-based disk electrostatic trap

As shown in Fig. 1, the octopole-based disk electrostatic trap (ODET) composes of two parallel disk electrodes with radii of 10 mm separated by 18 mm in the middle and eight cylindrical rods around forming an octopole with an inner radius of 13 mm. The disk electrode has a width of 2 mm and a hole with a radius of 2 mm in the center. The octopole elec-

trode is 30 mm long and has a radius of 3 mm. The first hole in the disk electrode allows molecules to enter and the second to extract the ions produced in the detection stage.

As shown in Fig. 2(a), when applying voltages of 0, $+U$, and $-U$ to the first disk electrode, the second one, and the octopole (each of the eight electrodes), respectively, a loading configuration is formed, in which the incident slow molecule in low-field-seeking (LFS) states will experience a negative dipolar force, resulting in standstill near the center of the trap. When the voltage of the first disk electrode is switched from 0 to $+U$ and the voltages of the other electrodes remain unchanged, a trapping configuration is formed, in which the loaded LFS state molecules will be confined, as shown in Fig. 2(b).
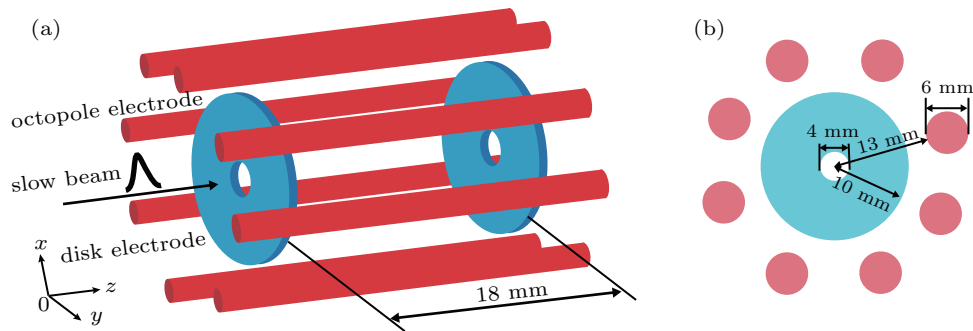

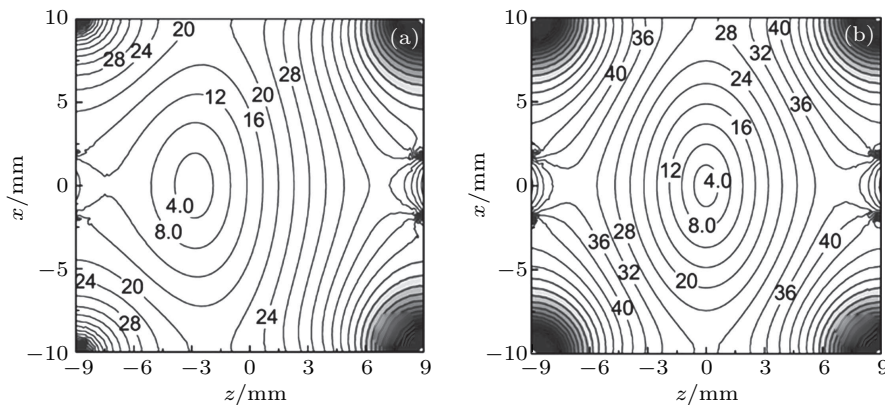**Fig. 1.** (a) Schematic diagram of the ODET. (b) The side view of the trap.

Fig. 2. The electric field distributions of the ODET in the x–z plane (a) under the loading configuration with $U = 26$ kV and (b) under the trapping configuration. The labels in the figure are all in units of kV/cm.

2.2. Tubular-based disk electrostatic trap

As to the tubular-based disk electrostatic trap (TDET), it has the same disk electrodes in size and layout as those of ODET, and a tubular electrode around, as shown in Fig. 3.
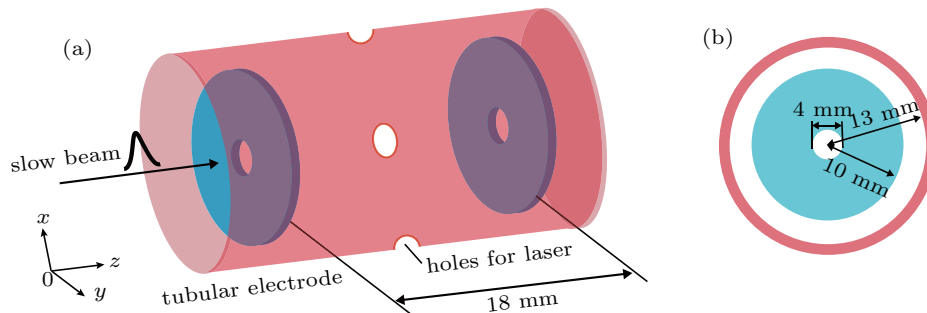

Fig. 3. (a) Schematic diagram of the TDET. (b) The side view of the trap.

The tubular electrode is 30 mm long and has an inner radius of 13 mm, a thickness of 2 mm. Two pairs of 5-mm-diameter holes are made in the middle part of the tubular electrode for laser detections along the x and y directions, respectively. When applying voltages of 0, $+U$, and $-U$ to the first disk electrode, the second one, and the tubular electrode, respectively, a loading configuration is formed, as shown in Fig. 4(a). When the voltage of the first disk electrode is switched from 0 to $+U$ and the voltages of the other electrodes stay the same, a trapping configuration is formed, as shown in Fig. 4(b).
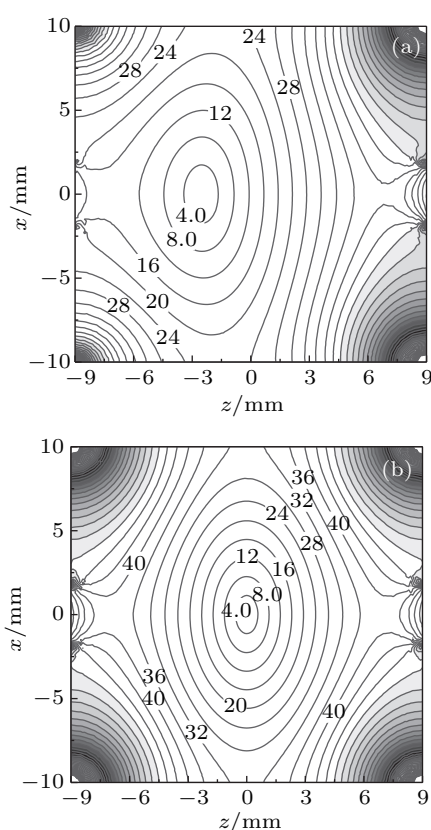

Fig. 4. The electric field distributions of the TDET in the x–z plane (a) under the loading configuration with $U = 26$ kV and (b) under the trapping configuration. The labels in the figure are all in units of kV/cm.

To get a detailed understanding of the two electrostatic traps (ODET and TDET), we calculate the electric field distributions along the z direction, i.e., the longitudinal direction, and the x direction, i.e., the transverse direction, under the loading and the trapping configurations with $U = 26$ kV, respectively. As shown in Fig. 5(a), the two dashed curves represent the electric field distributions of ODET (the blue one) and TDET (the red one) along the z direction under the loading configurations; the two solid curves show the electric field distributions of ODET (the blue one) and TDET (the red one) under the trapping configurations. Under the loading configurations, each trap has a potential hill in front of the trap center, a minimal point of electric field strength, and a rising electric field after the point. The minimal electric field strength

is not zero, but about 0.7 kV/cm and 0.4 kV/cm located at $z = -2.8$ mm and -2.5 mm in ODET and TDET, respectively. Generally, the incident molecules arriving at the minimal point start to climb up the rising potential and come to a standstill near or after the trap center, which means that the steeper rising field results in more reduction of the kinetic energy of the molecule. Under the trapping configurations, each trap has a minimal electric field strength at the trap center, also not zero, but nearly 0.7 kV/cm and 0.6 kV/cm at $z = 0$ in ODET and TDET, respectively. The nonzero fields are beneficial to avoid Majorana transitions in which the LFS state molecules might project onto the high-field-seeking (HFS) states and escape from the trap.[47] The trapping field distribution is symmetric along the trap center $z = 0$ in each trap. The trap depth is 34.1 kV/cm in ODET and 37.8 kV/cm in TDET. In Fig. 5(b), the two solid curves show the electric field distributions of ODET (the blue one) and TDET (the red one) along the transverse direction under the trapping configurations, respectively. The field distribution along the other transverse direction, the y direction, is not presented, as it is essentially the same as that along the x direction. The trap depth is 27.0 kV/cm in ODET and 30.5 kV/cm in TDET.

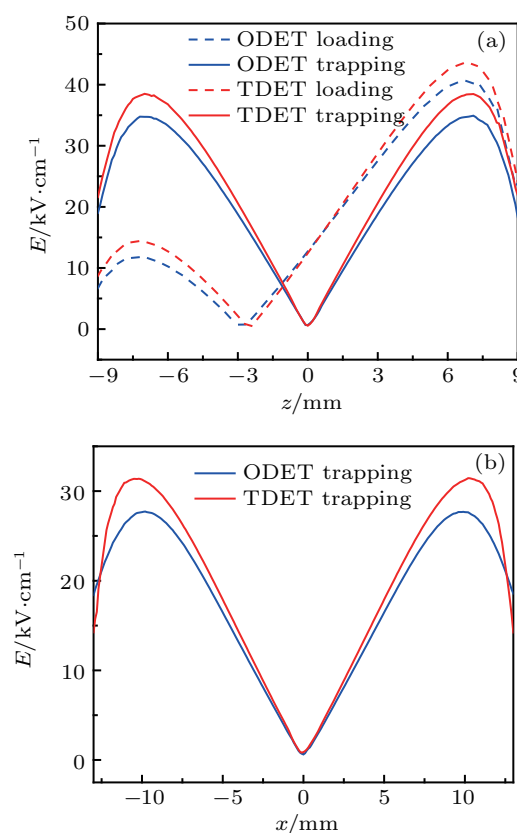**Fig. 5.** (a) The electric field distributions of ODET and TDET along the z direction, i.e., the longitudinal direction, under the loading configurations (the dashed curves) and the trapping configurations (the solid curves), with $U = 26$ kV. (b) The electric field distributions of ODET (the blue curve) and TDET (the red curve) along the x direction, i.e., the transverse direction, under the trapping configurations.

3. Loading methods and Monte Carlo simulations

3.1. Stark shifts of MgF molecules and the dipolar force

The slow MgF molecular beam with tunable central velocities can be achieved using a Stark decelerator.[48–51] Because the rotational temperature of the molecular beam after the supersonic expansion is usually several Kelvins and most of the molecules reside in the lowest rotational states, the Stark shifts of MgF molecules in the lowest rotational states are calculated, as shown in Fig. 6. MgF in $|1,1\rangle$ state is in the HFS state in the electric field and cannot be decelerated in the Stark decelerator. The molecule in $|1,0\rangle$ state has a turning point of 35 kV/cm after which the molecule converts into a HFS state. The molecule in $|2,2\rangle$ or $|2,1\rangle$ state turns to a HFS state in a weak field. The molecule in $|2,0\rangle$ state has a turning point of 101 kV/cm. Throughout the following simulations, MgF molecules in $|2,0\rangle$ state are used.
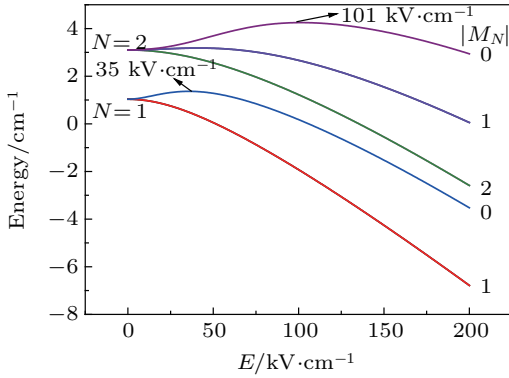

Fig. 6. The Stark shifts of MgF molecules in $N = 1, 2$ rotational states.

The dipolar force exerted on the dipolar molecule arises from the interaction between the molecular dipole moment and the applied electric field, which is the so called Stark effect. The dipolar force can be expressed as

$$F(r) = -\nabla W_S(r) = -(\mathrm{d}W_S/\mathrm{d}E)\nabla|E(r)|, \qquad (1)$$

where $F(r)$ is the dipolar force, $W_S(r)$ is the molecular Stark potential, $-(\mathrm{d}W_S/\mathrm{d}E)$ is the effective dipole moment, and $\nabla|E(r)|$ is the electric field gradient. MgF molecules in LFS states will experience a repulsive dipolar force when climbing the potential hill of the electrostatic trap under the loading configuration, and this is the force we employ to load the trap with MgF molecules.

3.2. Single loading and multi-loading of MgF molecules

In the numerical simulations, the selected molecule from the decelerated MgF molecular beam flies into the trap through the hole of the first disk electrode in the absence of the electric field. Once the molecule arrives at the minimal electric field under the loading configuration, the trap is switched into the

loading configuration. Then, the molecule starts to climb up the potential and is decelerated by the repulsive dipolar force. When the molecule is slowed to a standstill, the trap is switched into the trapping configuration, and then the molecule is confined in the trap. In this paper, we assume that the voltage applied to the trap is $U = 26$ kV and the incident pulsed MgF molecular beam has Gaussian distributions both in the spatial and velocity coordinates. The full widths at half maximum (FWHM) of the spatial and the velocity distributions in the x, y, and z directions are 4 mm, 4 mm, 6 mm and 5 m/s, 5 m/s, 6.5 m/s, respectively. The molecular number of one pulsed slow beam is 10^5. In addition, the elastic collisions are neglected in the simulations, because the density of the trapped molecules is not too high to lead to many collisions.

3.3. Simulation results in ODET

Using the single loading method, the trap is loaded with one pulsed molecular beam and the trapping configuration is kept till the end. The calculated trap loading efficiency is defined as the fraction of the one pulsed incident molecules, 10^5, and the molecules that are confined in the trap for 40 ms after the trapping configuration has been switched on. In Fig. 7, the dependence of the trap loading efficiency of ODET for MgF molecules on the incident velocity of the beam under the single loading operation mode (the black solid curve) is given. The loading efficiency increases with the increasing incident velocity, then it decreases with the increasing incident velocity above 10 m/s. Too low incident velocity causes more losses of molecules during the free-flying stage and too high incident velocity brings about more escapes of molecules from the trap potential, either of which leads to a decrease in the loading efficiency. When the incident velocity is 10 m/s, a highest loading efficiency of 78.4% is achieved.

With the multi-loading method, the trap is loaded with the first pulsed molecular beam under the loading configuration and switched into the trapping configuration upon finishing the loading process. Then, the trapping configuration is kept till the beginning of the loading and trapping for the second pulse. The duration of one loading and trapping cycle is 100 ms. When loading the second pulse, the trap requires opening up and switching back into the loading configuration, followed by the trapping process. In all, the processes repeat five times for five pulsed molecular beams. The loading efficiency is defined as the ratio of the molecules confined in the trap after the multi-loading to the molecules in one pulsed incident beam.[42] In Fig. 7, the dependence of the trap loading efficiency of ODET for MgF molecules on the incident velocity of the beam under the multi-loading operation mode (the red solid curve) is shown. With an incident velocity of 10 m/s, a highest loading efficiency of 99.9% is obtained, increasing by more than 27% in the number of the trapped molecules

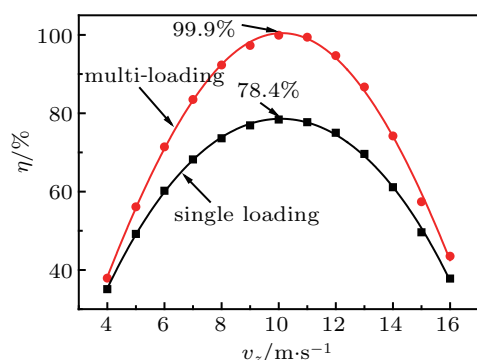comparing with that under the single loading operation mode.

Fig. 7. Dependences of the loading efficiency of the ODET for MgF molecules on the incident velocity of the slow beam under the single loading and the multi-loading operation modes, respectively.

With an incident velocity of 10 m/s in the slow beam, the phase-space distributions and the corresponding velocity distributions are presented, as shown in Fig. 8. The upper four sets of results in the figure are obtained under the single loading operation mode. The longitudinal phase-space distribution and the corresponding velocity distribution are shown in Figs. 8(a) and 8(b), respectively; the transverse phase-space distribution and the corresponding velocity distribution are shown in Figs. 8(c) and 8(d). Because the phase space and the velocity distributions of the trapped molecules in the y direction are the same as those in the x direction, the distributions in the y direction are not presented. The FWHMs of the velocity distributions of the trapped molecules in the z and x directions are about 18.4 m/s and 5.8 m/s, corresponding to the temperatures of 318 mK and 32 mK, respectively. In Fig. 8(a), the longitudinal phase-space distribution is highly structured, which is alternately empty and filled. In the center of the distribution, only a small number of molecules can be found. The

highly structured phase-space distribution was also found in the simulation of the traditional Stark deceleration.[52] In the first trapping experiments of OH radicals, the similar longitudinal phase-space distribution appeared when a pulsed molecular beam was loaded into an electrostatic trap with an actually too high velocity.[31] With a high incident velocity, the molecular beam spreads out less during the trap loading, which reduces the losses of molecules significantly, but the molecules only come to a standstill past the center of the trap. This leads to a donut-shape longitudinal phase-space distribution basically filling the entire trapping volume, as shown in Fig. 8(a), and a corresponding bimodal velocity distribution, as shown in Fig. 8(b). The transverse velocity distribution in Fig. 8(d) is almost a Gaussian with a single peak.

The lower four sets of results in Fig. 8 are obtained under the multi-loading operation mode. The longitudinal phase-space distribution and the corresponding velocity distribution are shown in Figs. 8(e) and 8(f), respectively; the transverse phase-space distribution and the corresponding velocity distribution are shown in Figs. 8(g) and 8(h). The FWHMs of the velocity distributions of the trapped molecules in the z and x directions are about 19.5 m/s and 5.8 m/s, corresponding to the temperatures of 357 mK and 32 mK, respectively. In Fig. 8(e), the longitudinal phase-space distribution also has an empty center similar to that in Fig. 8(a), but no other empty rings. The transverse velocity distribution in Fig. 8(h) is similar to that in Fig. 8(d) and also a Gaussian with a single peak.

Compared with the temperatures of the trapped MgF molecules under the single loading operation mode, the longitudinal temperature under the multi-loading operation mode increases by about 12%, still on the same order of magnitude, and the transverse temperature remains unchanged.
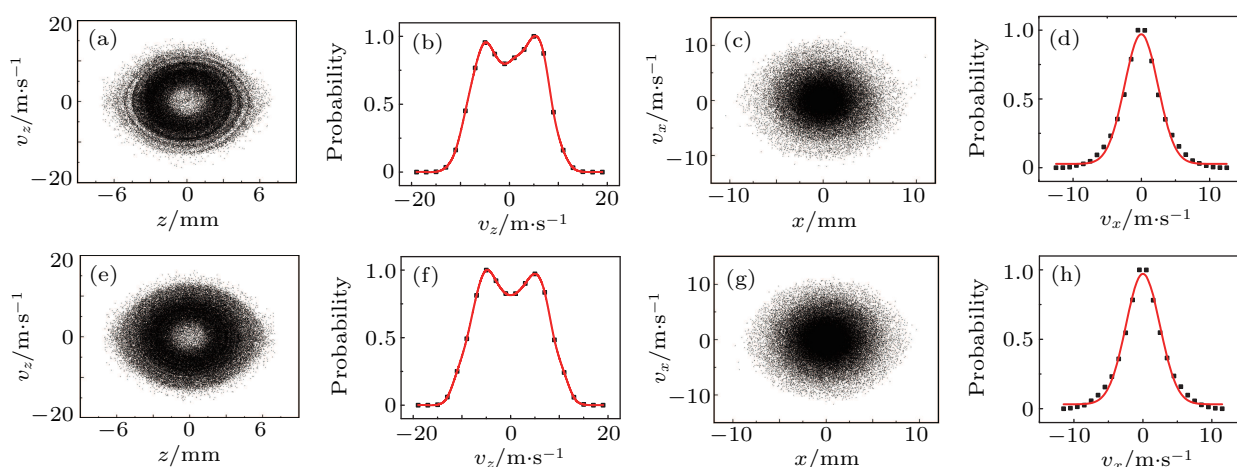

Fig. 8. The phase space and the velocity distributions of the trapped MgF molecules in the ODET while the highest loading efficiency is achieved with an incident velocity of 10 m/s, under (a)–(d) the single loading and (e)–(h) the multi-loading operation modes, respectively.

With an incident velocity of 7 m/s in the slow beam, the phase-space distributions and the corresponding velocity distributions are presented in Fig. 9. The upper four sets and the

lower four sets of results in the figure are obtained under the single loading and the multi-loading operation modes, respectively. Under the single loading operation mode, the FWHMs

of the velocity distributions of the trapped molecules in the z and x directions are about 12.4 m/s and 5.8 m/s, corresponding to the temperatures of 144 mK and 32 mK. Under the multi-loading operation, the FWHMs of the velocity distributions of the trapped molecules in the z and x directions are about 13.7 m/s and 5.9 m/s, corresponding to the temperatures of 176 mK and 33 mK.

In Fig. 9(a) or 9(e), the empty center disappears, compared with the distribution in Fig. 8(a) or 8(e). The basically Gaussian longitudinal velocity distribution with zero central velocity implies that the incident molecules with a velocity of 7 m/s come to a standstill at the trap center. The FWHM of the transverse velocity distribution is rather similar to that obtained with a higher loading velocity of 10 m/s. Mean-

while, the FWHM of the longitudinal velocity distribution obtained here, i.e., 12.4 m/s (with the single loading method) or 13.7 m/s (with the multi-loading method), is obviously smaller than that obtained with the loading velocity of 10 m/s, i.e., 18.4 m/s (with the single loading method) or 19.5 m/s (with the multi-loading method), which indicates that the trapped molecules with a lower temperature can be achieved with an appropriate lower incident velocity. On the other hand, trap loading with a lower incident velocity of 7 m/s leads to a lower loading efficiency which is 68.2% under the single loading operation mode or 83.5% under the multi-loading operation mode, compared with the loading efficiency 78.4% or 99.9% given an incident velocity of 10 m/s, as shown in Fig. 7.
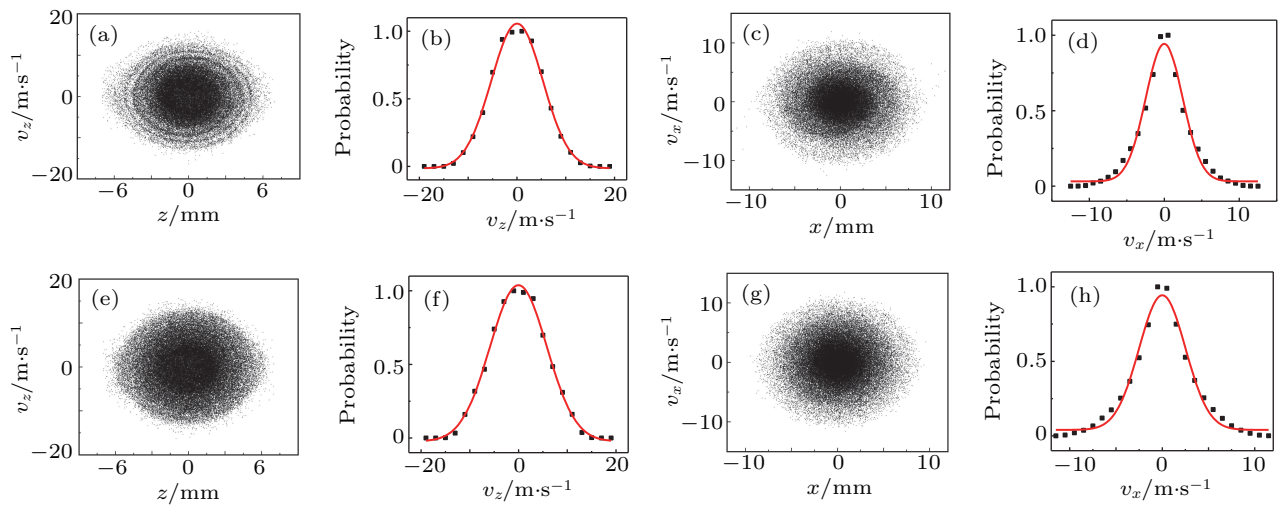

Fig. 9. The phase space and the velocity distributions of the trapped MgF molecules in the ODET with an incident velocity of 7 m/s, under (a)–(d) the single loading and (e)–(h) the multi-loading operation modes, respectively.

3.4. Simulation results in TDET

The definition of the loading efficiency of TDET is the same as that for ODET in Subsection 3.3. Figure 10 shows the dependence of the trap loading efficiency of TDET for MgF molecules on the incident velocity of the beam under the single loading (the black solid curve) and the multi-loading (the red solid curve) operation modes, respectively. When the incident velocity is 11 m/s, under the single loading operation mode, a highest loading efficiency of 81.6% is achieved; under the multi-loading operation mode, the loading efficiency amounts to 106.5%, increasing by 30% in the number of the trapped molecules comparing with that under the single loading operation mode.

Under the single loading or multi-loading operation mode, the phase-space distributions and the corresponding velocity distributions of the trapped MgF molecules in TDET are similar to those in ODET. When the highest loading efficiency is achieved, the FWHMs of the longitudinal velocity distributions of the trapped molecules in TDET are both about 1.4 times the FWHMs obtained in ODET, under the single loading and the multi-loading operation modes, respectively;

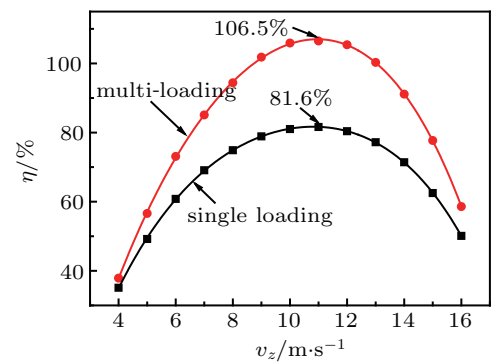the FWHM of the transverse velocity distribution in TDET is nearly the same as that in ODET.

Fig. 10. Dependences of the loading efficiency of the TDET for MgF molecules on the incident velocity of the beam under the single loading and the multi-loading operation modes, respectively.

4. Discussion

Compared with the disk electrostatic trap (DET) in Ref. [27], the ODET and TDET proposed here achieve a significant improvement in the trap loading efficiency. Using MgF as the target molecule, the dependences of the trap load-

ing efficiencies of DET, ODET, and TDET on the incident velocity of the slow beam under the single loading operation mode are calculated, respectively, as shown in Fig. 11, in which the blue and red solid curves are the same as the black solid curves in Figs. 7 and 10 and remain here for comparison only. Applying the same voltages on the electrodes of DET as those used in Ref. [27], i.e., voltages of 30 kV and 50 kV to the first and second disk electrodes in the loading configuration and voltages of 50 kV and 50 kV in the trapping configuration, a highest loading efficiency of 25.8% is obtained with an incident velocity of 6 m/s. Meanwhile, applying voltages of $U = 26$ kV to ODET (or TDET), a highest loading efficiency of 78.4% (or 81.6%) is achieved with an incident velocity of 10 m/s (or 11 m/s), resulting in an increase by a factor of two in the number of the trapped molecules.
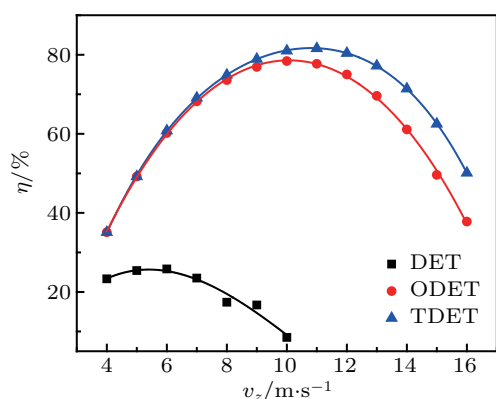

Fig. 11. The loading efficiencies of the DET, ODET, and TDET for MgF molecules at different incident velocities of the slow molecular beams under the single loading operation mode.

5. Conclusion

We have proposed two new electrostatic traps with simple construction and high loading efficiencies for cold polar molecules in LFS states. Under the trapping configuration, the voltage on the octopole electrodes of ODET or the tubular electrode of TDET significantly increases the transverse trap depth and effectively avoids the losses of molecules. This leads to a very high loading efficiency for each of the new traps. The multi-loading method proposed here is a simple versatile reloading method applicable for pulsed polar molecular packets of different species and explored with Monte Carlo simulations. With MgF as the target molecule, in ODET a highest loading efficiency of 78.4% or 99.9% has been achieved under the single loading operation or the multi-loading operation mode, and a highest loading efficiency of 81.6% or 106.5% has been achieved in TDET. The new electrostatic traps offer good early-stage preparations for the following gradient-intensity cooling of MgF molecules with a blue-detuned hollow beam, which may provide a new approach to produce dense ultracold molecules.

References

[1] Carr L D, DeMille D, Krems R V and Ye J 2009 *New J. Phys.* **11** 055049
[2] Bell M T and Softley T P 2009 *Mol. Phys.* **107** 99
[3] van de Meerakker S Y, Bethlem H L, Vanhaecke N and Meijer G 2012 *Chem. Rev.* **112** 4828
[4] Gilijamse J J, Hoekstra S, van de Meerakker S Y, Groenenboom G C and Meijer G 2006 *Science* **313** 1617
[5] Sawyer B C, Stuhl B K, Yeo M, Tscherbul T V, Hummon M T, Xia Y, Kłos J, Patterson D, Doyle J M and Ye J 2011 *Phys. Chem. Chem. Phys.* **13** 19059
[6] Stuhl B K, Hummon M T and Ye J 2014 *Annu. Rev. Phys. Chem.* **65** 501
[7] Kirste M, Wang X, Schewe H C, Meijer G, Liu K, van der Avoird A, Janssen L M, Gubbels K B, Groenenboom G C and van de Meerakker S Y 2012 *Science* **338** 1060
[8] Krems R V 2008 *Phys. Chem. Chem. Phys.* **10** 4079
[9] Bell M T, Gingell A D, Oldham J M, Softley T P and Willitsch S 2009 *Faraday Discuss.* **142** 73
[10] Berteloite C, Lara M, Bergeat A, Le Picard S D, Dayou F, Hickson K M, Canosa A, Naulin C, Launay J M Sims I R and Costes M 2010 *Phys. Rev. Lett.* **105** 203201
[11] Narevicius E and Raizen M G 2012 *Chem. Rev.* **112** 4879
[12] van Veldhoven J, Küpper J, Bethlem H L, Sartakov B, van Roij A J and Meijer G 2004 *Eur. Phys. J. D* **31** 337
[13] Hudson E R, Lewandowski H, Sawyer B C and Ye J 2006 *Phys. Rev. Lett.* **96** 143004
[14] Hudson J J, Sauer B E, Tarbutt M R and Hinds E A 2002 *Phys. Rev. Lett.* **89** 023003
[15] Collaboration A C M E 2014 *Science* **343** 269
[16] Cairncross W B, Gresh D N, Grau M, Cossel K C, Roussy T S, Ni Y, Zhou Y, Ye J and Cornell E A 2017 *Phys. Rev. Lett.* **119** 153001
[17] Shafer-Ray N E, Milton K A, Furneaux B R, Abraham E and Kalbfleisch G R 2003 *Phys. Rev. A* **67** 045401
[18] van Veldhoven J, Bethlem H L and Meijer G 2005 *Phys. Rev. Lett.* **94** 083001
[19] van Veldhoven J, Bethlem H L, Schnell M and Meijer G 2006 *Phys. Rev. A* **73** 063408
[20] Schnell M, Lützow P, Van Veldhoven J, Bethlem H L, Küpper J, Friedrich B, Schleier-Smith M, Haak H and Meijer G 2007 *J. Phys. Chem. A* **111** 7411
[21] Sawyer B C, Lev B L, Hudson E R, Stuhl B K, Lara M, Bohn J L and Ye J 2007 *Phys. Rev. Lett.* **98** 253002
[22] Kirste M, Sartakov B G, Schnell M and Meijer G 2009 *Phys. Rev. A* **79** 051401
[23] Meek S A, Conrad H and Meijer G 2009 *Science* **324** 1699
[24] Gilijamse J J, Hoekstra S, Vanhaecke N, van de Meerakker S Y and Meijer G 2010 *Eur. Phys. J. D* **57** 33
[25] Li S Q, Xu L, Xia Y, Wang H L and Yin J P 2014 *Chin. Phys. B* **23** 123701
[26] Wang Z X, Gu Z X, Deng L Z and Yin J P 2015 *Chin. Phys. B* **24** 053701
[27] Sun H, Wang Z X, Wang Q, Li X J, Liu J P and Yin J P 2015 *Chin. Phys. B* **24** 113101
[28] Weinstein J D, DeCarvalho R, Guillet T, Friedrich B and Doyle J M 1998 *Nature* **395** 148
[29] Takekoshi T, Patterson B M and Knize R J 1998 *Phys. Rev. Lett.* **81** 5105
[30] Bethlem H L, Berden G, Crompvoets F M, Jongma R T, Van Roij A J and Meijer G 2000 *Nature* **406** 491
[31] van de Meerakker S Y, Smeets P H, Vanhaecke N, Jongma R T and Meijer G 2005 *Phys. Rev. Lett.* **94** 023004
[32] Gilijamse J J, Hoekstra S, Meek S A, Metsälä M, van de Meerakker S Y, Meijer G and Groenenboom G C 2007 *J. Chem. Phys.* **127** 221102
[33] Hoekstra S, Metsälä M, Zieger P C, Scharfenberg L, Gilijamse J J, Meijer G and van de Meerakker S Y 2007 *Phys. Rev. A* **76** 063408
[34] Campbell W C, Tsikata E, Lu H I, van Buuren L D and Doyle J M 2007 *Phys. Rev. Lett.* **98** 213001
[35] Tsikata E, Campbell W, Hummon M, Lu H I and Doyle J M 2010 *New J. Phys.* **12** 065028
[36] van de Meerakker S Y, Vanhaecke N, van der Loo M P, Groenenboom G C and Meijer G 2005 *Phys. Rev. Lett.* **95** 013003
[37] Sawyer B C, Stuhl B K, Wang D, Yeo M and Ye J 2008 *Phys. Rev. Lett.* **101** 203203

[38] Hummon M T, Tscherbul T V, Kłos J, Lu H I, Tsikata E, Campbell W C, Dalgarno A and Doyle J M 2011 *Phys. Rev. Lett.* **106** 053201

[39] Stuhl B K, Yeo M, Hummon M T and Ye J 2013 *Mol. Phys.* **111** 1798

[40] Zeppenfeld M, Englert B G, Glöckner R, Prehn A, Mielenz M, Sommer C, van Buuren L D, Motsch M and Rempe G 2012 *Nautre* **491** 570

[41] van de Meerakker S Y, Jongma R T, Bethlem H L and Meijer G 2001 *Phys. Rev. A* **64** 041401

[42] Riedel J, Hoekstra S, Jäger W, Gilijamse J J, van de Meerakker S Y and Meijer G 2011 *Eur. Phys. J. D* **65** 161

[43] Rieger T, Junglen T, Rangwala S A, Pinkse P W and Rempe G 2005 *Phys. Rev. Lett.* **95** 173002

[44] Kang S, Gao Y, Kuang F, Gao T, Du J and Jiang G 2015 *Phys. Rev. A* **91** 042511

[45] Xu L, Yin Y, Wei B, Xia Y and Yin J 2016 *Phys. Rev. A* **93** 013408

[46] Xu S, Xia M, Yin Y, Gu R, Xia Y and Yin J 2019 *J. Chem. Phys.* **150** 084302

[47] Harland P W, Hu W P, Vallance C and Brooks P R 1999 *Phys. Rev. A* **60** 3138

[48] Van den Berg J E, Mathavan S C, Meinema C, Nauta J, Nijbroek T H, Jungmann K, Bethlem H L and Hoekstra S 2014 *J. Mol. Spectrosc.* **300** 22

[49] Hou S, Wang Q, Deng L and Yin J 2016 *J. Phys. B: At. Mol. Opt. Phys.* **49** 065301

[50] Wang Q, Hou S, Xu L and Yin J 2016 *Phys. Chem. Chem. Phys.* **18** 5432

[51] Shyur Y, Bossert J A and Lewandowski H J 2018 *J. Phys. B: At. Mol. Opt. Phys.* **51** 165101

[52] van de Meerakker S Y, Vanhaecke N, Bethlem H L and Meijer G 2006 *Phys. Rev. A* **73** 023401